Simon Kamel[1]
Department of Mechanical Engineering,
Imperial College London,
London SW7 2AZ, UK
e-mail: s.kamel@ic.ac.uk

Noel P. O'Dowd
Department of Mechanical and Aeronautical Engineering,
Materials and Surface Science Institute,
University of Limerick,
Limerick, Ireland
e-mail: noel.odowd@ul.ie

Kamran M. Nikbin
Department of Mechanical Engineering,
Imperial College London,
London SW7 2AZ, UK
e-mail: k.nikbin@ic.ac.uk

Evaluation of Two-Parameter Approaches to Describe Crack-Tip Fields in Engineering Structures

The application of two-parameter approaches to describe crack-tip stress fields has generally focused on Ramberg–Osgood (RO) power law material behavior, which limits the range of applicability of such approaches. In this work we consider the applicability of a J-Q or J-A_2 approach (the latter is designated here as the J-A approach) to describe the stress fields for RO power law materials and for a material whose tensile behavior is not described by a RO model. The predictions of the two-parameter approaches are compared with full field finite-element predictions. Results are presented for shallow and deep-cracked tension and bend geometries, as these are expected to provide the expected range of constraint conditions in practice. A new approach for evaluating Q is proposed for a RO material, which, for a given geometry, makes Q dependent only on the strain hardening exponent. [DOI: 10.1115/1.3120266]

Keywords: fracture, constraint, elastic-plastic, finite-element analysis, crack-tip fields

1 Introduction

Under conditions of low crack-tip constraint, J-dominance is lost and the crack-tip fields may no longer be characterized by a single parameter. Thus two or more parameters are required to provide an accurate representation of crack-tip fields under low constraint conditions. Two such parameters, which have received considerable attention in literature, are the hydrostatic Q parameter [1,2] and the A_2 parameter for a power law material [3–5]. Numerical studies of these parameters have generally focused on Ramberg–Osgood (RO) power law hardening material behavior, which, in practice, is often not representative of engineering materials. In this paper we evaluate the ability of two-parameter approaches to describe the crack-tip stress fields for RO power law hardening behavior and for a material whose tensile behavior is not completely described by the RO model. For the latter we consider X100 pipeline steel, a high strength carbon steel with relatively low-strain hardening. We have focused our study on center cracked tension M(T) and single edge notch bend SEN(B) geometries, with a/W of 0.1, 0.4, and 0.7 as these are considered to cover the range of crack-tip constraint expected in engineering structures. The predictions are compared with the full field finite-element (FE) crack-tip stress distributions, with differences quantified using an error parameter to provide an evaluation of these two-parameter approaches.

2 Background to Two-Parameter Approaches

2.1 *J-Q* Approach. From finite-element analyses of cracked geometries, the difference between the Hutchinson, Rice, and Rosengren (HRR) fields [6,7] and the finite-element stress fields was found in Ref. [1] to be approximately a uniform hydrostatic stress over the microstructurally significant region ahead of the crack tip. This feature was observed for tension geometries and bend geometries under low deformation. The uniformity of the hydrostatic stress was found to be better satisfied when the difference was taken with respect to the stress field from a finite-element small scale yielding (SSY) solution with $T=0$, where T is the linear elastic T-stress [8]. Accordingly Q was defined in Ref. [2] from the equation

$$\sigma_{ij} = (\sigma_{ij})_{\mathrm{SSY};T=0} + Q\sigma_0 \tag{1}$$

where σ_0 is an appropriately defined normalizing stress, typically the yield stress.

2.2 *J-A* Approach. Using an asymptotic mathematical analysis, a three-term solution was developed [3–5] to characterize the mode-I crack-tip fields for a crack in a RO power law hardening material described by

$$\frac{\varepsilon}{\varepsilon_0} = \frac{\sigma}{\sigma_0} + \alpha\left(\frac{\sigma}{\sigma_0}\right)^n \tag{2}$$

where α is the "yield offset," n is the strain hardening exponent, σ_0 is a normalizing stress, which is usually related to the yield stress, and $\varepsilon_0=\sigma_0/E$ where E is Young's modulus. The crack-tip stress fields in a polar coordinate system (r,θ) are given by

$$\frac{\sigma_{ij}}{\sigma_0} = \left(\frac{J}{\alpha\varepsilon_0\sigma_0 I_n r}\right)^{1/(n+1)} \tilde{\sigma}_{ij}^{\mathrm{HRR}}(\theta) + A\left(\frac{J}{\alpha\varepsilon_0\sigma_0 I_n L}\right)^{1/(n+1)}\left(\frac{r}{L}\right)^s \tilde{\sigma}_{ij}^{(1)}(\theta) + A^2\left(\frac{J}{\alpha\varepsilon_0\sigma_0 I_n L}\right)^{1/(n+1)}\left(\frac{r}{L}\right)^t \tilde{\sigma}_{ij}^{(2)}(\theta) \tag{3}$$

where J is Rice's J-integral [9], and the angular functions $\tilde{\sigma}_{ij}^{(k)}$, the stress power exponents s and t, and the dimensionless integration constant I_n depend only on n. (Note that slightly different notation from that used in the earlier work [5,10] has been employed in Eq. (3). In particular, the symbol A is used here in place of A_2.) The parameter L in Eq. (3) is a characteristic, normalizing length parameter, which in previous work has been chosen as the crack length a, the specimen width W, the thickness B, or unity [5,10]. Note that for a given stress distribution, the value obtained for A will depend on the choice of characteristic length L, but the overall amplitude of the stress field is unaffected.

Plane strain mode-I dimensionless functions $\tilde{\sigma}_{ij}^{(k)}$, I_n, and the exponents s and t have been tabulated in Ref. [11]. It may be seen from Eq. (3) that if $A=0$ the equation reduces to the HRR field. Thus, J describes the amplitude of the HRR field and A characterizes the "loss of constraint", which results in a reduction in stress magnitude relative to the HRR field.

[1]Corresponding author.

Contributed by the Pressure Vessel and Piping Division of ASME for publication in the JOURNAL OF PRESSURE VESSEL TECHNOLOGY. Manuscript received September 26, 2007; final manuscript received December 24, 2008; published online April 21, 2009. Review conducted by T. L. (Sam) Sham. Paper presented at the 2007 ASME Pressure Vessels and Piping Conference (PVP2007), San Antonio, TX, July 22–26, 2007.

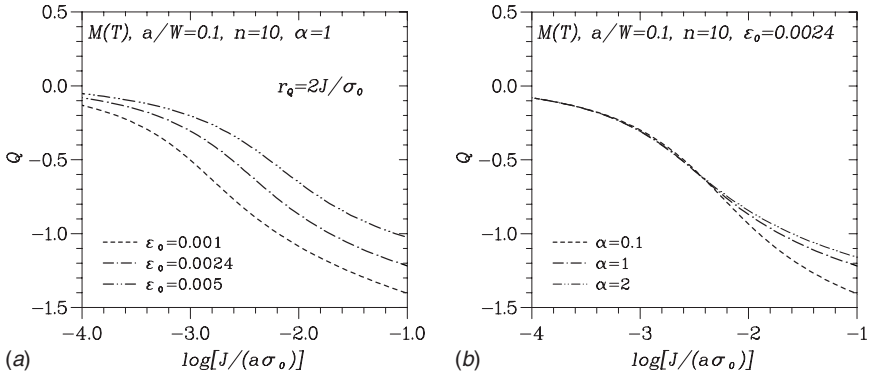

Fig. 1 ***Q*** **versus** $J/a\sigma_0$ **for a range of values of (*a*)** ε_0 **and (*b*)** α**, where** ***Q*** **is evaluated at the normalized distance** $\bar{r}=2$

3 Evaluating *Q* From Finite-Element Solutions

3.1 Conventional Evaluation of *Q*. The constraint parameter Q is conventionally evaluated at a fixed normalized distance ahead of the crack tip $\bar{r}$ given by

$$\bar{r} = r_Q/(J/\sigma_0) \tag{4}$$

where r_Q is the physical distance from the crack tip at which Q is evaluated. Typically $\bar{r}$ is in the range $1<\bar{r}<5$, which is the microstructurally significant range over which stresses and strains control the fracture process. This can be interpreted in terms of the crack-tip opening displacement (CTOD) δ_t, which is defined in Ref. [12] as the relative displacement of the crack faces at a distance from the crack tip at which 45 deg lines emanating from the crack tip intersect with the crack faces. In Ref. [12] it was shown that under small scale yielding conditions the CTOD can be linearly related to J/σ_0 by

$$\delta_t = d_n \frac{J}{\sigma_0} \tag{5}$$

where d_n is defined via the HRR field as

$$d_n = (\alpha\varepsilon_0)^{1/n}\tilde{d}_n \tag{6}$$

and $\tilde{d}_n$ is given by

$$\tilde{d}_n = \frac{2\tilde{u}_y(n)}{I_n}[\tilde{u}_x(n)+\tilde{u}_y(n)]^{1/n} \tag{7}$$

where $\tilde{u}_x(n)$ and $\tilde{u}_y(n)$ are dimensionless constants obtained from the HRR field and are dependent on n. For materials of interest, d_n is typically in the range $0.2<d_n<0.7$.

Clearly, by combining Eqs. (4) and (5), we can write that

$$r_Q = \left(\frac{\bar{r}}{d_n}\right)\delta_t \tag{8}$$

Taking an average value for d_n of 0.5, it follows that if the range of evaluation for Q is over the region $1<\bar{r}<5$, in terms of CTOD this is $2\delta_t<r_Q<10\delta_t$.

One of the difficulties associated with evaluating Q at the normalized distance $\bar{r}$ is that there will be a dependence on the material parameters ε_0 and α, as discussed in Ref. [13]. The dependence of Q on ε_0 and α, for example, is shown in Fig. 1 for M(T), $a/W=0.1$ with $n=10$. Here Q is evaluated at a distance $r_Q=2J/\sigma_0$, $(\bar{r}=2)$, and J is normalized by $a\sigma_0$. The dependence of Q on ε_0 and, to a lesser extent on α, complicates the compilation of handbook solutions for Q for a RO material. Below we propose an approach for eliminating the dependence on α and ε_0. This considerably simplifies the tabulation of Q for a given geometry, as Q is then dependent only on n.

3.2 Alternative Definition for Constraint Parameter *Q*. The RO model (Eq. (2)) is defined using four parameters, α, ε_0, σ_0, and n, (note that, by definition, $E=\sigma_0/\varepsilon_0$, and is not an additional parameter in the material description). Defining the material model in this ways allows flexibility in the choice of material parameters, e.g., σ_0 can be chosen as the 0.2% flow stress with ε_0 the corresponding strain. However, as pointed out in Refs. [13,14], a RO material model is *fully* determined using only three material parameters, so that Eq. (2) may be rewritten as

$$\frac{\varepsilon}{\hat{\varepsilon}_0} = \frac{\sigma}{\hat{\sigma}_0} + \left(\frac{\sigma}{\hat{\sigma}_0}\right)^n \tag{9}$$

where the normalizing stress and strain, $\hat{\sigma}_0$ and $\hat{\varepsilon}_0$, respectively, are given as

$$\hat{\sigma}_0 = \sigma_0/\alpha^{1/(n-1)} \tag{10a}$$

$$\hat{\varepsilon}_0 = \varepsilon_0/\alpha^{1/(n-1)} \tag{10b}$$

Note that $\hat{\sigma}_0/\hat{\varepsilon}_0=\sigma_0/\varepsilon_0=E$ (provided $n>1$). Equations (2) and (9) provide identical representations of a RO material—if material data are fitted using Eq. (2) (in terms of α, ε_0, and σ_0), the fit can be equivalently represented as Eq. (9), with $\hat{\sigma}_0$ and $\hat{\varepsilon}_0$ defined using Eq. (10). The normalizing stress $\hat{\sigma}_0$ can no longer be identified directly with a particular level of inelastic strain, but from Eq. (9), it may be seen that if $\sigma<\hat{\sigma}_0$, the material response is in the linear regime and if $\sigma>\hat{\sigma}_0$, the power law term dominates.

In an analysis of a material that obeys Eq. (9), results will depend only on the power law exponent n provided stresses are normalized by $\hat{\sigma}_0$ and strain quantities by $\hat{\varepsilon}_0$; see e.g., discussion in Ref. [14]. Thus, an appropriate dimensionless distance $\hat{r}$ may be defined as

$$\hat{r} = r_Q/(J/\hat{\varepsilon}_0\hat{\sigma}_0) \tag{11}$$

and Eq. (1) may be rewritten as

$$\sigma_{ij} = (\sigma_{ij})_{\mathrm{SSY};T=0} + Q\hat{\sigma}_0 \tag{12}$$

By evaluating Q using the dimensionless distance $\hat{r}$, and normalizing J by $a\hat{\varepsilon}_0\hat{\sigma}_0$, the resultant J-Q plot will be independent of $\hat{\varepsilon}_0$ and $\hat{\sigma}_0$ and depend only on n (for a given geometry). For example, all the lines in Fig. 1 collapse onto a single line, as shown in Fig. 2, when normalized appropriately. A different value for Q will be obtained if Eq. (12) is used rather than Eq. (1), due to the different choice of normalizing stress ($\hat{\sigma}_0$ rather than σ_0) and a different choice of dimensionless distance (through $\hat{\varepsilon}_0$). This issue will be discussed in more detail later. Note that if $\alpha=1$, then $\hat{\varepsilon}_0=\varepsilon_0$ and $\hat{\sigma}_0=\sigma_0$.

3.3 Choice of Normalizing Distance. Having defined the normalized distance $\hat{r}$ in Eq. (11), an appropriate value of $\hat{r}$ at

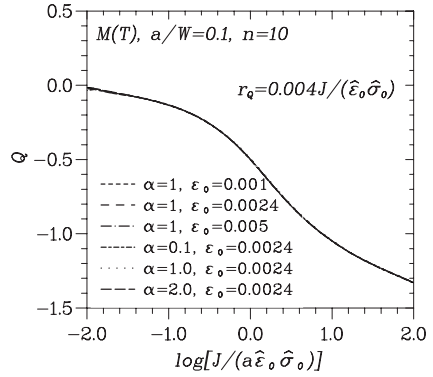

Fig. 2 Variation of Q versus $J/a\hat{\varepsilon}_0\hat{\sigma}_0$ for a range of values of ε_0 and α, where Q is evaluated at the normalized distance $\hat{r}=0.004$

which Q is evaluated must be chosen. Equation (12) indicates that the second term in the J-Q-representation of the crack-tip fields is independent of distance and thus the same value for Q would be obtained regardless of the position where it is evaluated. However, Eq. (12) is an approximation and, in practice, the value obtained for Q will show some dependence on the distance at which it is evaluated. The value of $\hat{r}$ should be chosen so that the physical distance r_Q in Eq. (11) is at some appropriate fraction of δ_t, such that Q is evaluated over a microstructurally significant distance. Using Eqs. (5), (6), and (11), the distance r_Q can be shown to be related to the crack-tip opening displacement δ_t by

$$r_Q = \frac{1}{\hat{\varepsilon}_0^{(n+1)/n}}\left(\frac{\hat{r}}{\tilde{d}_n}\right)\delta_t \tag{13}$$

where $\tilde{d}_n$ has been defined in Eq. (7).

In this work we have chosen to evaluate Q at a normalized distance $\hat{r}=0.004$, which corresponds to a distance of $4\delta_t$ for the case of $n=10$, $\alpha=1$, and $\varepsilon_0=0.002$ (i.e., $\hat{\varepsilon}_0=0.002$). Thus, in terms of the physical distance from the crack tip, Q is evaluated at a position

$$r_Q = \frac{1}{\hat{\varepsilon}_0^{(n+1)/n}}\left(\frac{0.004}{\tilde{d}_n}\right)\delta_t \tag{14}$$

This is the point at which Q is evaluated for the cases shown in Fig. 2.

It may be noted that if r_Q is defined using the conventional definition, Eq. (8), for low hardening materials the $r_Q-\delta_t$ relationship depends weakly on $\hat{\varepsilon}_0$ (a $1/n$ dependence through Eq. (6)) and choosing $\bar{r}=2$ will generally ensure that Q is evaluated at a physically representative distance. However, Eq. (14) indicates that for low hardening materials, r_Q/δ_t is more strongly dependent on $\hat{\varepsilon}_0$ ($(n+1)/n \to 1$). Thus, to ensure that r_Q falls within the range $2\delta_t < r_Q < 10\delta_t$, limits must be placed on the value of $\hat{\varepsilon}_0$. The applicable ranges of $\hat{\varepsilon}_0$ are obtained from Eq. (15) and for convenience have been grouped into three sets of values of n, i.e.,

$$2\times10^{-3} < \hat{\varepsilon}_0 < 6\times10^{-3} \quad \text{for} \quad 3 \le n \le 4$$

$$1.5\times10^{-3} < \hat{\varepsilon}_0 < 4\times10^{-3} \quad \text{for} \quad 4 < n \le 7$$

$$1\times10^{-3} < \hat{\varepsilon}_0 < 3\times10^{-3} \quad \text{for} \quad n > 7 \tag{15}$$

As long as n and $\hat{\varepsilon}_0$ lie within these limits, Q will be evaluated in the range $2\delta_t < r_Q < 10\delta_t$, i.e., at a microstructurally significant distance. It is expected that most materials commonly encountered in engineering applications will lie within the limits of applicability given in Eq. (15). If $\hat{\varepsilon}_0$ is outside these limits, it is recommended that Q is evaluated directly from FE analysis with an appropriate definition of the normalizing distance.

In summary, in this work the parameter Q is determined as the difference between the normal stress σ_{22} from a finite-element analysis and the value of σ_{22} obtained from a SSY boundary analysis with $T/\hat{\sigma}_0=0$, at a normalized distance of $r_Q/J/(\hat{\varepsilon}_0\hat{\sigma}_0)=0.004$. If a RO model is defined using Eq. (2) (i.e., in terms of α, ε_0, and σ_0) Q values may still be obtained from Fig. 2 with $\hat{\sigma}_0$ and $\hat{\varepsilon}_0$ defined via Eq. (9).

In previous work [1,2], Q was evaluated at the distance $r_Q/(J/\sigma_0)=2$. For $\alpha=1$ and $\varepsilon_0=E/\sigma_0=500$, this distance is equivalent to the distance $\hat{r}=0.004$. However, for other materials, the new normalized distance is not equivalent to $r/(J/\sigma_0)=2$. Since Q will have a (weak) dependence on distance, it is expected that there will be some differences in Q values evaluated at the new normalized distance and previously published values. Furthermore, since a different normalizing stress, $\hat{\sigma}_0$, has been used in Eq. (12) rather than σ_0, this will affect the value of Q. This issue is discussed further in Sec. 6.3.

4 Evaluation of the Constraint Parameter, A

To allow direct comparison of the J-Q and J-A approaches we rewrite the J-A stress field in Eq. (3) in terms of $\hat{\sigma}_0$ and $\hat{\varepsilon}_0$ as follows:

$$\frac{\sigma_{ij}}{\hat{\sigma}_0} = \left(\frac{J}{\hat{\varepsilon}_0\hat{\sigma}_0 I_n r}\right)^{1/(n+1)}\tilde{\sigma}_{ij}^{\mathrm{HRR}}(\theta) + A\left(\frac{J}{\hat{\varepsilon}_0\hat{\sigma}_0 I_n r}\right)^{1/(n+1)}\left(\frac{r}{L}\right)^{[s(n+1)+1]/(n+1)}\tilde{\sigma}_{ij}^{(1)}(\theta) + A^2\left(\frac{J}{\hat{\varepsilon}_0\hat{\sigma}_0 I_n r}\right)^{1/(n+1)}\left(\frac{r}{L}\right)^{[t(n+1)+1]/(n+1)}\tilde{\sigma}_{ij}^{(2)}(\theta) \tag{16}$$

Following the approach in Ref. [15], the value of A is determined from a finite-element analysis using the "weight averaging method." This entails equating the average finite-element stress between defined limits, to the integral of Eq. (16) between the same limits of $\hat{r}$, i.e.,

$$\int_{\hat{r}_1}^{\hat{r}_2}\sigma_{\mathrm{FE}}d\hat{r} = \int_{\hat{r}_1}^{\hat{r}_2}\sigma_{J\text{-}A}d\hat{r} \tag{17}$$

where $\sigma_{J\text{-}A}$ is the stress field in Eq. (16) and σ_{FE} is the normal (σ_{22}) FE stress distribution. In Ref. [15], A is evaluated in the range $1<\bar{r}<5$. Here we have taken the range to be $0.002<\hat{r}<0.01$, which is equivalent to the range taken in Ref. [15] when $n=10$, and $\alpha=1$ and $\varepsilon_0=0.002$, and is consistent with the evaluation of Q at $\hat{r}=0.004$.

By substituting Eq. (16) into the right-hand side of Eq. (17), and evaluating the integrals, it follows that the value of A can be determined by solving the quadratic equation

$$xA^2 + yA + z = 0 \tag{18}$$

where x, y, and z are given by

$$x = \tilde{\sigma}_{ij}^{(2)}\left(\frac{J}{\hat{\varepsilon}_0\hat{\sigma}_0 L}\right)^t\frac{0.01^{t+1}-0.002^{t+1}}{t+1}$$

$$y = \tilde{\sigma}_{ij}^{(1)}\left(\frac{J}{\hat{\varepsilon}_0\hat{\sigma}_0 L}\right)^s\frac{0.01^{s+1}-0.002^{s+1}}{s+1}$$

$$z = \tilde{\sigma}_{ij}^{(\mathrm{HRR})}\left(\frac{J}{\hat{\varepsilon}_0\hat{\sigma}_0 L}\right)^{-1/(n+1)}(0.01^{n/(n+1)} - 0.002^{n/(n+1)})\frac{n+1}{n} - \left(\frac{J}{\hat{\varepsilon}_0\hat{\sigma}_0 I_n L}\right)^{-1/(n+1)}\int_{0.002}^{0.01}\frac{\sigma_{\theta\theta}^{\mathrm{FE}}(\hat{r},0)}{\hat{\sigma}_0}d\hat{r} \quad (19)$$

The characteristic length L has been taken as the crack length a in all calculations.

For comparison, we have also evaluated A by equating the J-A stress field in Eq. (16) to the FE stress at $\hat{r}=0.004$ (the same distance at which Q has been evaluated). The value of A obtained from the two methods is almost identical.

5 Finite-Element Procedures

5.1 Analyses Performed. Center cracked panels under tension, designated M(T), and edge cracked bend specimens, designated SEN(B), have been analyzed. The dimensions of the M(T) specimens are $H/W=2$ for $a/W=0.1$, and $H/W=4$ for $a/W=0.4$ and 0.7, where H is the total height and W is half the width of the plate. The total span S of the SEN(B) specimens is $S=4W$. The results are expected to be independent of specimen height, H/W, and S/W and depend only on a/W. The loading for the SEN(B) is applied as three point bending with S the distance between the support points. Due to symmetry, only a quarter of the M(T) plate and a half of the SEN(B) geometry are modeled.

The finite-element analyses were performed using ABAQUS 6.6 [16], with a small displacement formulation. The RO material analyses were performed using deformation plasticity whereas the analyses for X100 test data used incremental plasticity. It was found, however, that the difference in the results between the two plasticity models is negligible for a small displacement formulation. Four noded two-dimensional plane strain elements (ABAQUS element type CPE4H) were used in all cases. The finite-element meshes were generated with a sharp crack, the crack-tip element size ranging from $\sim 10^{-5}a$ to $10^{-3}a$, in order to provide detailed stress distributions at different deformation levels.

5.2 Evaluation of Error for the Two-Parameter Predictions. To provide a quantitative measure of how well the J-A or J-Q approach describes the crack-tip stress distributions, we have defined a dimensionless error parameter e as

$$e = \frac{\int_{\hat{r}_1}^{\hat{r}_2}|\sigma_{\mathrm{FE}} - \sigma_P|d\hat{r}}{\int_{\hat{r}_1}^{\hat{r}_2}\sigma_{\mathrm{FE}}d\hat{r}} \quad (20)$$

where σ_{FE} is the finite-element stress, σ_P is the J-A- or J-Q-prediction, and $\hat{r}_1$ and $\hat{r}_2$ are the limits over which the error is calculated. This parameter gives the average magnitude of the difference between the finite-element stress distribution and the two-parameter prediction, as a ratio of the average magnitude of the finite-element stress. The error e is evaluated over a chosen range of $\hat{r}$, which in this work has been taken to be $0.004<\hat{r}<0.01$.

6 Analyses of RO Power Law Materials

In this section we assess the ability of the J-A- and J-Q approaches to characterize the crack-tip stress fields for materials that behave according to the RO material model. Analyses were performed for two values of strain hardening exponent, $n=5$ and $n=10$, in order to simulate high and moderate hardening materials, respectively. The results provided can be used for any value of $\hat{\sigma}_0$ and $\hat{\varepsilon}_0$ but care should be taken in interpreting the results if $\hat{\varepsilon}_0$ falls outside the applicability limits given in Eq. (15). The values of the stress power exponents, s and t, the dimensionless integration constant, I_n, and the mode-I angular stress distributions, $\tilde{\sigma}_{ij}^{(k)}$ at $\theta=0$, are given in Tables 1 and 2 (the data for $n=5$, 10, and 15 are taken from Ref. [11], and the data for $n=25$ are extrapolated values).

Table 1 Stress exponents (s and t) and integration constants (I_n) for evaluation of A, and values of $(\sigma_{22}/\hat{\sigma}_0)_{\mathrm{SSY};T=0}$ reference stress field for evaluation of Q

n	s	t	I_n	$(\sigma_{22}/\hat{\sigma}_0)_{\mathrm{SSY};T=0;\hat{r}=4\times10^{-3}}$
5	0.05456	0.27578	5.024	3.85
10	0.06977	0.2304	4.540	3.37
15	0.06093	0.18435	4.334	–
25	0.0458[a]	0.130[a]	4.134[a]	–

[a]These values are obtained by extrapolation.

6.1 Predictions of Normal (σ_{22}) Stress Distributions. Figure 3 shows the normal stress distributions $\sigma_{22}/\hat{\sigma}_0$ for a shallow-cracked M(T) geometry under extensive plasticity, for $n=10$. The normalizing load $\hat{P}_0$ is the plane strain limit load given in Ref. [17], with σ_0 replaced with $\hat{\sigma}_0$, i.e.,

$$\hat{P}_0 = \frac{4Bb}{\sqrt{3}}\hat{\sigma}_0 \quad (21)$$

where B is the thickness, and b is the width of the ligament$=W-a$. It can be seen in Fig. 3 that both the J-A and J-Q approaches provide a good prediction of the normal stress distribution in the M(T) geometry over the microstructurally significant range $0.002<\hat{r}<0.01$. The J-Q approach gives a somewhat better prediction than the J-A-prediction (this result is representative of the deep-cracked M(T) cases and the shallow-cracked ($a/W=0.1$) SEN(B) case).

The results for the deep-cracked SEN(B) geometry are presented in Fig. 4 for a normalized load of $P/\hat{P}_0=1.6$. Here $\hat{P}_0$ is the plane strain limit load for a SEN(B) geometry [17], with σ_0 replaced with $\hat{\sigma}_0$, i.e.,

Table 2 Angular stress values $\tilde{\sigma}_{ij}^{(k)}$ (at $\theta=0$) for evaluation of A

n	$\tilde{\sigma}_{ij}^{\mathrm{HRR}}$	$\tilde{\sigma}_{ij}^{(1)}$	$\tilde{\sigma}_{ij}^{(2)}$
5	2.2171	0.3184	−3.2224
10	2.4969	0.313	−6.4128
15	2.6162	0.2975	−7.8432
25	2.730[a]	0.273[a]	−10.87[a]

[a]These values are obtained by extrapolation.

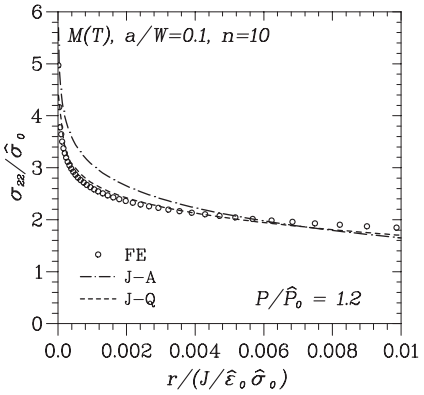

Fig. 3 Normal stress distributions ahead of the crack tip for an M(T) geometry, $a/W=0.1$, and $n=10$, at a load $P=1.2\hat{P}_0$

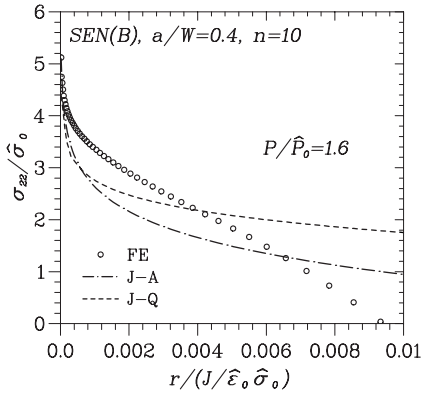

Fig. 4 Normal stress distributions ahead of the crack tip for a SEN(B) geometry, $a/W=0.4$, and $n=10$, at a load $P=1.6\hat{P}_0$

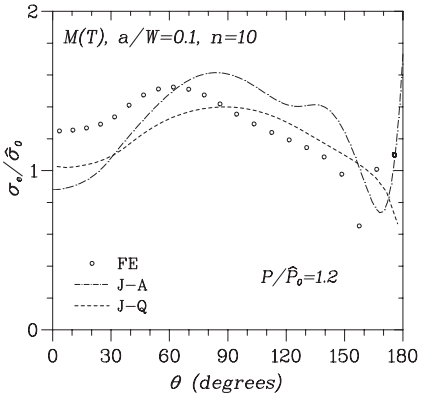

Fig. 7 Angular variation of equivalent von Mises stress for M(T), $a/W=0.1$, at a load of $1.2\hat{P}_0$

$$\hat{P}_0 = \frac{1.409Bb^2\hat{\sigma}_0}{S} \tag{22}$$

For this case, both the *J-A* and *J-Q* approaches give poor predictions. The result is consistent with those presented in Refs. [1,10]—the poor agreement with the crack-tip field solutions arises from the fact that the global bending stress impinges on the crack-tip fields at large deformation. The result in Fig. 4 is also representative of the SEN(B) $a/W=0.7$ case.

Figures 5 and 6 show the error e defined in Eq. (20), plotted against the normalized load, for the shallow-cracked M(T), and deep-cracked SEN(B) geometries, respectively. It can be seen from Fig. 5 that the error e for the M(T) geometry is less than 5% up to the maximum load shown. Similar magnitudes of e were found for the deep-cracked M(T) cases, and the shallow-cracked SEN(B). The value of e for the deep-cracked SEN(B) case is shown in Fig. 6, from which it can be seen that e increases very rapidly beyond a load of $\sim 1.2\hat{P}_0$, due to the effect of the global bending stress on the crack-tip field. A similar trend was seen for $a/W=0.7$. Thus, the use of the *J-A* or *J-Q*-approach does not significantly extend the applicability of *J*-based fracture mechanics to deeply cracked bend specimens when loads are considerably in excess of the plastic collapse load ($P>1.4\hat{P}_0$).

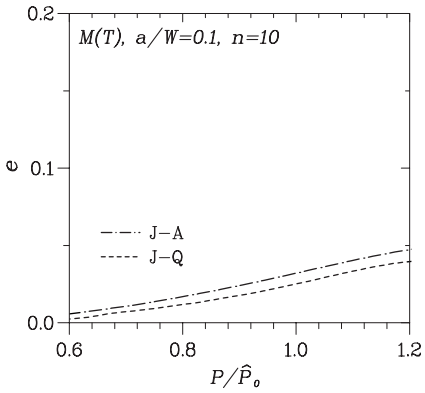

Fig. 5 Error e versus normalized load for an M(T) geometry, $a/W=0.1$, and $n=10$

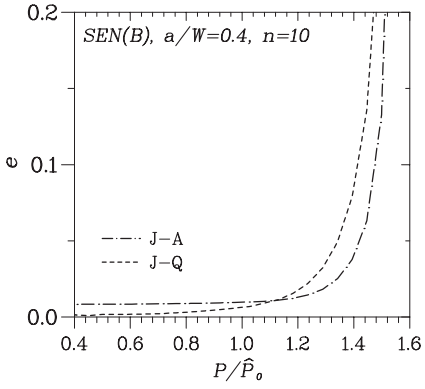

Fig. 6 Error e versus normalized load for a SEN(B) geometry, $a/W=0.4$, and $n=10$

6.2 Prediction of von Mises Equivalent Stress. In this section, we compare the von Mises equivalent stress (σ_e) distributions predicted by the *J-Q* and *J-A* approaches for 2D plane strain.

For the *J-A* approach, the in-plane stress components σ_{22} and σ_{11}, and the shear stress σ_{12} are calculated from Eq. (16), where the angular functions $\bar{\sigma}_{ij}^{(1)}$ and $\bar{\sigma}_{ij}^{(2)}$ are taken from Ref. [11] and A is obtained using the procedure described in Sec. 4. The out-of-plane component σ_{33} is given by $\sigma_{33}=0.5(\sigma_{11}+\sigma_{22})$. The *J-Q* approach uses the von Mises equivalent stress based on the SSY analysis.

The angular variation of equivalent stress is shown in Fig. 7 for the shallow-cracked M(T), $a/W=0.1$, and $n=10$, for a load of $1.2\hat{P}_0$, under large scale plasticity. It may be seen that both the *J-Q* and *J-A* approaches give reasonable predictions. A similar trend was seen for $n=5$.

6.3 Discussion of the Alternative Normalizing Distance. For a RO power law material, the use of the alternative normalizing distance $\hat{r}=0.004$ should give a similar σ_{22} (normal) stress distribution, as the conventional normalizing distance $\bar{r}=2$. This implies that $Q\sigma_0$ in Eq. (1) should be approximately equal to $Q\hat{\sigma}_0$ in Eq. (12). A measure of the difference in the stress fields obtained using the two normalizing distances has been obtained by plotting the ratio $\Delta S'/\Delta S$ against normalized load, where $\Delta S = Q\sigma_0$ and $\Delta S' = Q\hat{\sigma}_0$. This ratio has been plotted in Fig. 8 for the shallow-cracked M(T) and deeply cracked SEN(B), representative of, respectively, low constraint and high constraint conditions. A value of $\Delta S'/\Delta S=1$ indicates that the predictions of the stress field given by the two normalizations are identical. For each geometry, the error is presented for $n=5$ and $n=10$, and a range of values of ε_0 and α. Note that Q is evaluated within the range $2 < r/\delta_t < 10$ for all cases.

For the M(T) geometry, $0.9 \le \Delta S'/\Delta S \le 1.1$ for $n=10$, and less than 1.25 for $n=5$. The value of $\Delta S'/\Delta S$ for the SEN(B), $a/W=0.4$, geometry is somewhat larger; at the lowest load shown, the lowest value of $\Delta S'/\Delta S$ is 0.7. Note, however, that at this load

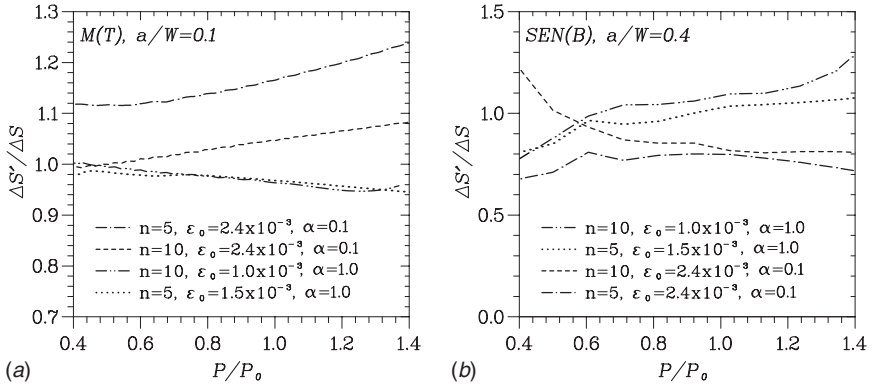

Fig. 8 $\Delta S'/\Delta S$ versus normalized load $P/\hat{P}_0$ for (*a*) M(T), $a/W=0.1$, and (*b*) SEN(B), $a/W=0.4$, geometries

level, $Q \simeq 0$, thus $\Delta S'$ and ΔS are also approximately zero. A more appropriate measure of the error at low load is the ratio of the total stress predicted using the alternative and conventional normalizing distances, which in this case is less than 1%. At the largest load shown, $P=1.4P_0$, the value of $\Delta S'/\Delta S$ is 1.3. This difference is considered to be reasonable in view of the effect of the global bending stress on the crack-tip fields at this load level as indicated in Fig. 4.

The definition of Q proposed in the current paper is based on the normalizing stress $\hat{\sigma}_0$. If values of Q are available based on the normalizing stress σ_0 in the standard form of the RO law (Eq. (1)), the value of Q obtained using the current normalization may be estimated as

$$Q_{\text{new}} = \frac{(\sigma_{ij})_{\text{SSY};T=0} - (\hat{\sigma}_{ij})_{\text{SSY};T=0} + Q\sigma_0}{\sigma_0} \tag{23}$$

where Q_{new} indicates the Q value obtained using the current normalization and $(\sigma_{ij})_{\text{SSY};T=0}$ and $(\hat{\sigma}_{ij})_{\text{SSY};T=0}$ indicate the reference stress obtained using σ_0 and $\hat{\sigma}_0$, respectively. Note that Eq. (23) does not include the effect of matching distance on Q and only accounts for the effect of normalizing stress. Our FE studies show that the maximum difference in Q values obtained using either definition is 38%, for both the shallow-cracked M(T) and deep-cracked SEN(B) geometries.

7 Analyses of a Real Material: X100 Pipeline Steel

In practice, engineering materials do not behave according to the RO power law. Since the *J-A* approach is based on the RO model, however, it is necessary to fit the RO model to the material stress-strain curve in order to apply the approach. The *J-Q* approach can be applied to any material behavior.

In this section we examine a low hardening, ferritic steel (X100), which is used predominantly in oil and gas pipeline applications. The finite-element stress distributions obtained from these analyses are then compared with the *J-A*-prediction obtained by performing the analyses using a RO model fit to the data, as well as the *J-Q*-prediction based on the analyses using the tensile test data.

The available stress-strain data give Young's modulus of 211 GPa and a 0.2% proof stress of ~640 MPa [18]. Q is determined at $\hat{r}=0.004$, where $\hat{\sigma}_0=\sigma_{0.2}$ (0.2% proof stress) and $\hat{\varepsilon}_0=\hat{\sigma}_0/E$, so $\hat{\varepsilon}_0=\sigma_{0.2}/E$. The value of $(\sigma_{22}/\hat{\sigma}_0)_{\text{SSY};T=0}$ is 3.25.

7.1 RO Model Fits to The Tensile Test Data. Tensile data for the RO model are unavailable above ~8% strain; therefore the data were extrapolated based on the trend of the data before 8%. Two RO fits were made to the data, one to give a good fit in the low-strain region and the other at high strains. The values of the RO parameters for the fits are provided in Table 3. The comparison between the tensile data and the RO model fits is shown in Fig. 9. Figure 9(*a*) shows the fits over the low-strain region (up to 5% strain) and Fig. 9(*b*) shows the fit over the full range (up to 20% strain). It may be seen that fit *A* is close to the test data up to ~5%, while at strain levels above 5%, fit *B* provides a better fit to the data. Note that for both fits, $\hat{\sigma}_0/\hat{\varepsilon}_0=E=211$ GPa.

Table 3 RO model fits to ×100 tensile test data

	n	$\hat{\sigma}_0$	$\hat{\varepsilon}_0$
RO model fit *A*	15	667	3.16×10^{-3}
RO model fit *B*	25	718	3.41×10^{-3}

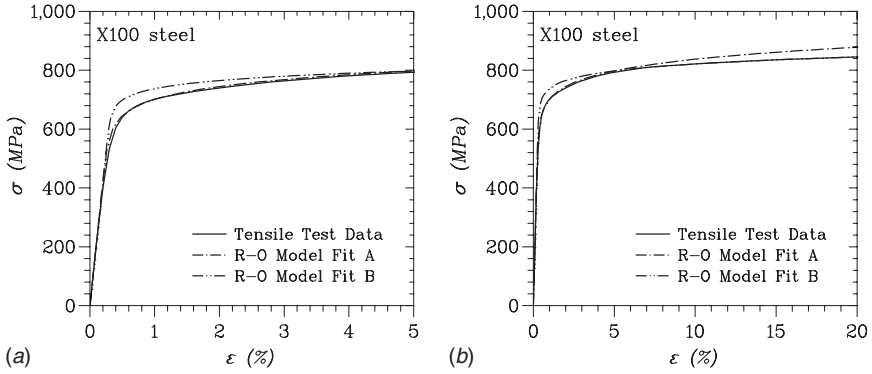

Fig. 9 True stress-strain curve for ×100 steel up to (*a*) 5% strain and (*b*) 20% strain

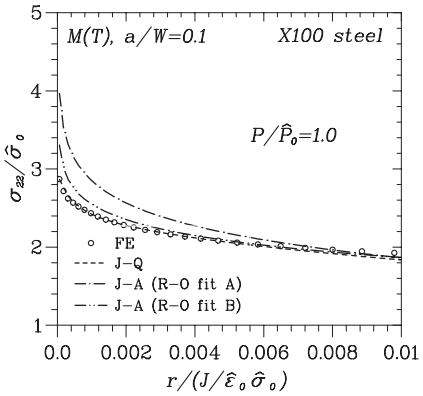

Fig. 10 Normal stress distributions ahead of the crack tip for an M(T) geometry, $a/W=0.1$, ×100 steel, at a load $P=1.0\hat{P}_0$

7.2 Comparison of Q and A Predictions for X100 Material. The values of A were obtained from the finite-element analyses following the procedure discussed in Sec. 4. The values of Q were obtained from a finite-element analysis using the tensile test data illustrated in Fig. 9. The values of A and Q were then inserted into the appropriate equation and the resultant stress distribution compared with the finite-element stress distribution obtained using the tensile test data.

Figures 10 and 11 show the normal stress distributions for, respectively, a shallow-cracked M(T), $a/W=0.1$, and a deep-cracked SEN(B), $a/W=0.4$, at a load $P=1.0\hat{P}_0$. It may be seen for both cases that the *J-Q*-predictions, obtained using the material tensile response, provide closer agreement with the full finite-element solution than the *J-A*-predictions, obtained using power law fits (the *J-Q*-predictions (dashed lines) are almost indistinguishable from the finite-element solution (open symbol)). For the M(T) specimen, the agreement from the *J-A*-prediction with RO fit *B* provides a closer agreement than that obtained using fit *A*. This is expected since the low constraint shallow-cracked M(T) case experiences high-strain levels, and thus at high load better agreement is obtained for the M(T) geometry using the high-strain fit (fit *B*).

The high constraint deep-cracked SEN(B) geometry in Fig. 11 experiences relatively low strain apart from very close to the crack tip. Thus it is expected that for the SEN(B) geometry, fit *A* (the low-strain fit) will provide better agreement with the finite-element stress fields than fit *B* over most of the crack-tip region. Close to the crack tip ($\hat{r}<0.002$), it may be seen in Fig. 11 that fit *B* provides close agreement to the finite-element prediction. However, this result is of limited significance as finite strain effects dominate within this region. Thus, for the SEN(B) geometry at this load level, better agreement is obtained over the region of interest using fit *A*.

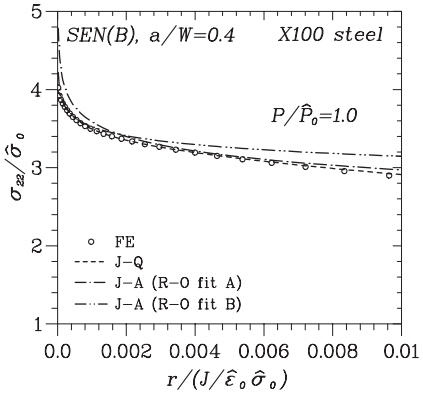

Fig. 11 Normal stress distributions ahead of the crack tip for a SEN(B) geometry, $a/W=0.4$, ×100 steel, at a load $P=1.0\hat{P}_0$

These results emphasize that care is needed in fitting the RO law to experimental data if one wishes to obtain an accurate prediction of crack-tip stresses, and an appropriate material fit for one geometry, load level, or distance may not be appropriate for another. (This conclusion applies to a *J-Q* or *J-A* approach if the tensile response is fitted with a RO model.)

8 Discussion and Conclusions

Finite-element analyses of shallow and deep-cracked M(T) and SEN(B) geometries have been performed in order to evaluate the ability of the *J-Q* and *J-A* approaches to describe the crack-tip fields, for both RO power law hardening materials and for a pipeline steel, whose tensile behavior is not described by the RO model. The constraint parameters are essentially equivalent if they are to be used to provide a constraint-based toughness locus as discussed in Refs. [2,5].

The analyses of the RO power law materials have shown that both the *J-A* and *J-Q* approaches give a good prediction of the normal (σ_{22}) stress fields for the shallow and deep-cracked M(T) geometries and for the shallow-cracked SEN(B) geometry. Perhaps surprisingly, the approximate *J-Q* approach gave a consistently better prediction than the asymptotic *J-A* approach. However, it should be noted that the *J-Q* approach requires a numerically calculated reference field, while the *J-A* approach uses the known HRR distribution as a reference field. For the deep-cracked SEN(B) geometry, both approaches were found to give a poor prediction under high loads, which is due to the fact that the global bending stress impinges on the crack-tip fields. The effect of the global bending stress on the crack-tip fields can be accounted for by including an additional term in the *J-Q* or *J-A* crack-tip field equations, as discussed in Refs. [19,20]. Both the *J-A* and *J-Q* approaches require either tabulated values of the parameters, J, A, and Q, or a finite-element analysis to obtain these parameters. If the *J-A* approach is being used, the exponents s and t, and the angular stress distributions $\tilde{\sigma}_{ij}^{(k)}$ must be available. A *J-Q* analysis requires the solution of the small scale yielding ($T/\hat{\sigma}_0=0$) solution for the material in question. For an engineering material, the *J-Q* approach has been found to give close agreement with the finite-element stress distribution for the material considered here, X100 pipeline steel. The applicability of the *J-A* distribution, however, is dependent on how well a RO model can be fitted to the material stress-strain curve.

In practice, it may not be feasible to tabulate Q values for all materials. Thus the use of a RO model is attractive, and values of Q for a particular geometry can be tabulated as only a function of power law exponent, n, when the normalization discussed in Sec. 3.2 is used.

Acknowledgment

Useful discussions with Dr C. M. Davies of Imperial College London are acknowledged.

References

[1] O'Dowd, N., and Shih, C., 1991, "Family of Crack-Tip Fields Characterized by a Triaxiality Parameter, Part I: Structure of Fields," J. Mech. Phys. Solids, **39**, pp. 989–1015.
[2] O'Dowd, N., and Shih, C., 1992, "Family of Crack-Tip Fields Characterized by a Triaxiality Parameter, Part II: Fracture Applications," J. Mech. Phys. Solids, **40**, pp. 939–963.
[3] Yang, S., Chao, Y., and Sutton, M., 1993, "Complete Theoretical Analysis for Higher Order Asymptotic Terms and the HRR Zone at a Crack Tip For Mode I and Mode II Loading of a Hardening Material," Acta Mech., **98**, pp. 79–98.
[4] Yang, S., Chao, Y., and Sutton, M., 1993, "Higher Order Asymptotic Crack Tip Fields in a Power-Law Hardening Material," Eng. Fract. Mech., **45**, pp. 1–20.
[5] Chao, Y., Yang, S., and Sutton, M., 1994, "On the Fracture of Solids Characterized by One or Two Parameters: Theory and Practice," J. Mech. Phys.

Solids, **42**, pp. 629–47.
[6] Hutchinson, J., 1968, "Singular Behaviour at End of Tensile Crack in Hardening Material," J. Mech. Phys. Solids, **16**, pp. 13–31.
[7] Rice, J., and Rosengren, G., 1968, "Plane Strain Deformation Near Crack Tip in Power-Law Hardening Material," J. Mech. Phys. Solids, **16**, pp. 1–12.
[8] Williams, M., 1957, "On Stress Distribution at Base of Stationary Crack," ASME J. Appl. Mech., **24**, pp. 109–114.
[9] Rice, J. R., 1968, "A Path Independent Integral and the Approximate Analysis of Strain Concentrations by Notches and Cracks," ASME J. Appl. Mech., **35**, pp. 379–386.
[10] Chao, Y., and Zhu, X., 1998, "J-A_2 Characterization of Crack-Tip Fields: Extent of J-A_2 Dominance and Size Requirements," Int. J. Fract., **89**, pp. 285–307.
[11] Chao, Y., and Zhang, L., 1997, "Tables of Plane Strain Crack Tip Fields: HRR and Higher Order Terms," Department of Mechanical Engineering, University of South Carolina, Technical Report No. ME-Report 97-1.
[12] Shih, C., 1981, "Relationships Between the J-Integral and the Crack Opening Displacement for Stationary and Extending Cracks," J. Mech. Phys. Solids, **29**, pp. 305–326.
[13] O'Dowd, N., 1995, "Applications of Two Parameter Approaches in Elastic-Plastic Fracture Mechanics," Eng. Fract. Mech., **52**, pp. 445–465.
[14] Härkegård, G., and Sørbø, S., 1998, "Applicability of Neuber's Rule to the Analysis of Stress and Strain Concentration Under Creep Conditions," ASME J. Eng. Mater. Technol., **120**, pp. 224–229.
[15] Chao, Y. J., Zhu, X. K., Lam, P. S., Louthan, M. R., and Iyer, N. C., 2000, "Application of the Two-Parameter J-A_2 Description to Ductile Crack Growth," *Fatigue and Fracture Mechanics, 31st Volume*, ASTM STP 1389, G. Halford and J. Gallagher, eds., American Society for Testing and Materials, Philadelphia, PA, pp. 165–182.
[16] Dassault Systémes Simulia Corp., 2006, ABAQUS version 6.6.
[17] British Energy, 2006, R6 Revision 4: Assessment of the Integrity of Structures Containing Defects.
[18] O'Dowd, N., and MacGillivray, H., 2003, "Study of Girth Welds at High Strains," Imperial College London, ICON Technical Report No. ME025/1.
[19] Zhu, X., and Leis, B., 2006, "Bending Modified J-Q Theory and Crack-Tip Constraint Quantification," Int. J. Fract., **141**, pp. 115–134.
[20] Chao, Y., Zhu, X., Kim, Y., Lar, P., Pechersky, M., and Morgan, M., 2004, "Characterization of Crack-Tip Field and Constraint for Bending Specimens Under Large-Scale Yielding," Int. J. Fract., **127**, pp. 283–302.